Chemicals

Bis(hexamethylene)triamine (143-23-7), nickel(II) chloride hexahydrate (99%, 7791-20-0), and dimethylglyoxime (97%, 95-45-4) were purchased from Sigma-Aldrich. Paraformaldehyde (96%, 30525-89-4) and hypophosphorous acid (50%, 6303-21-5) were purchased from Acros Organics. Sulfuric acid (96%, 7664-93-9), ethanol (96%, 64-17-5), ammonium hydroxide (25%, 1336-21-6) and hydrochloric acid (35–38%, 7647-01-0) were purchased from POCH.

Equipment

The image of the obtained amino-hypophosphite polyampholyte was taken using a JSM-6610LV scanning electron microscope (JEOL Ltd., Akishima, Japan) after sputtering the samples with carbon using a JEC-530 automatic coating machine (JEOL Ltd., Akishima, Japan). The specific surface area of this material was evaluated by research on sorption and desorption of the helium/nitrogen mixture using the FlowSorb 2300 apparatus (Micromeritics Instruments Corp, Norcross, GA, USA). The density of the resin obtained was measured using a pycnometer. XPS spectra were carried out using a multi-chamber UHV analytical system (Prevac, Poland) equipped with a hemispherical R4000 photoelectron energy analyser excited by monochromatic X-rays emitted by an MX-650 lamp with an Al-Kα anode (Gammadata Scienta, Sweden). The deconvolution and quantitative spectra analysis was performed using Casa XPS software (Casa Software Ltd., UK). The chemical composition of the applied wastewater was introduced into an ICP MS spectrometer (model 7500cx, Agilent, USA). An Evolution 201 UV-visible spectrophotometer (Thermo Fisher Scientific, Madison, USA) was used for spectrophotometric concentration measurements.

Table S1. The capacities of Ni(II) sorption on different sorbents as follows from the literature reports.

Sorbent	Sorption capacity (mg/g)	Isotherm model	Conditions	References
Amberlite IRA-458	65.24	Langmuir	initial Ni(II) concentration: 600 mg·dm^{-3} pH 4.0 temp. 20-60^{o}C sorbent dosage: 0.5 g	[1]
Amberlite IRA-958	53.16			
Amberlite IRA-67	13.19			
Dowex PSR-2	19.16	Langmuir	initial Ni(II) concentration: 100 mg·dm^{-3} temp. 20^{o}C contact time: 240 min sorbent dosage: 0.1 g agitation speed: 180 rpm	[2]
Dowex PSR-3	31.72			
Lewatit TP-207	1.23	N/A	initial Ni(II) concentration: 0.395 mg·dm^{-3} pH 6.0 contact time: 72 h sorbent dosage: 0.27 g·dm^{-3}	[3]
Lewatit AF-5	4.89	Freundlich	initial Ni(II) concentration: 100 mg·dm^{-3} temp. 25^{o}C contact time: 240 min sorbent dosage: 0.5 g agitation speed: 180 rpm	[4]
Lewatit MonoPlus SR-7	4.56	Freundlich	initial Ni(II) concentration: 100 mg·dm^{-3} temp. 25^{o}C contact time: 24 h	[5]
Lewatit MonoPlus TP-220	6.24	N/A	initial Ni(II) concentration: 100 mg·dm^{-3} sorbent dosage: 0.5 g agitation speed: 180 rpm ambient temperature	[6]
Cliniptilolite ion-exchange	3.28	Langmuir	Ni(II) concentration: 0.1–100 mg·dm^{-3}	[7]

resin			pH 7.0 sorbent dosage: 15 g·dm^{-3} agitation speed: 250 rpm contact time: 180 min	
Modified cliniptilolite	8.90	Langmuir	initial Ni(II) concentration: 50-900 mg·dm^{-3} pH 6.0 temp. 25^{o}C sorbent dosage: 100 g·dm^{-3} contact time: 300 min	[8]
Chitosan/cliniptilolite	247.0	Langmuir	initial Ni(II) concentration: 4109 mg·dm^{-3} pH 5.0 temp. 25^{o}C contact time: 24 h	[9]
Carboxymethyl chitosan-hemicellulose resin (CMCH)	362.3	Freundlich	initial Ni(II) concentration: 100 mg·dm^{-3} pH 6.0 temp. 25^{o}C contact time: 7 h	[10]
Glucan/chitosan hydrogel	184.0	Langmuir	pH 7.0 temp. 20^{o}C contact time: 2 h sorbent dosage: 0.01 g	[11]
Oxidised carbon nanotubes	49.26	Langmuir	Ni(II) concentration: 10–200 mg·dm^{-3}, sorbent dosage: 0.4 g·dm^{-3} pH 6.0	[12]
Multipore activated carbons	56.90	Langmuir	pH 6.0 temp. 30^{o}C contact time: 150 min sorbent dosage: 100 mg	[13]
Hydrophilic carbon nanoparticles over silica	13.48	Langmuir	initial Ni(II) concentration: 2.5 mg·dm^{-3} pH 4.0 temp. 20^{o}C	[14]

Mesoporous calcium silicate	278.35	N/A	initial Ni(II) concentration: 150 mg·dm^{-3} pH 5.0-7.5 temp. 25^{o}C contact time: 3 h	[15]
Acid treated montmorillonite	4.0	Langmuir	initial Ni(II) concentration: 2.04 mg·dm^{-3} pH 6.5 temp. 25^{o}C	[16]
Mixed layer clay	6.25	N/A	initial Ni(II) concentration: 100 mg·dm^{-3} pH 5.6 temp. 25^{o}C contact time: 100 min	[17]
Ball-milled South African bentonite clay	1.3	Freundlich	pH 6.0 temp. 26^{o}C contact time: 1 h	[18]
Barley straw ash	8.25	N/A	initial Ni(II) concentration: 16 mg·dm^{-3} pH 6.5 temp. 80^{o}C contact time: 1.5 h	[19]
Peanut husk powder	56.82	Langmuir	initial Ni(II) concentration: 20 mg·dm^{-3} pH 6.0 temp. 25^{o}C sorbent dosage: 5 g·dm^{-3}	[20]
Coconut husk	404.5	N/A	initial Ni(II) concentration: 200 mg·dm^{-3} pH 6.0 temp. 80^{o}C contact time: 40 min sorbent dosage: 1 g	[21]
Cd-H_4bta MOF	120.3	Langmuir	initial Ni(II) concentration: 100 mg·dm^{-3} temp. 25^{o}C contact time: 30 min	[22]
Magnetic nanorods	95.42	Langmuir	initial Ni(II) concentration: 200 mg·dm^{-3}	[23]

			pH 5.5 temp. 25°C	
Magnetic graphene oxide	51.02	Langmuir	initial Ni(II) concentration: 60 mg·dm^{-3} pH 8.0 temp. 25°C	[24]
Magnetite-Dowex 50WX4	384.0	Langmuir	initial Ni(II) concentration: 100 mg·dm^{-3} pH 7.0 temp. 25°C	[25]
Iron oxide magnetic nanoparticles grafted on hyperbranched polyglycerol	0.45	N/A	initial Ni(II) concentration: 100 mg·dm^{-3} pH 7.2 temp. 25°C	[26]

Table S2. Kinetic models and equilibrium isotherms used in this work

Models	Form of equation		Parameters	Reference
Pseudo-first-order equation (PFO)	$\log(q_{exp} - q_t) = \log(q_1) - \left(\frac{k_1}{2.303}\right) \cdot t$	(1)	q_1 (mmol g^{-1}) k_1 (min^{-1})	[27,28]
Pseudo-second-order equation (PSO)	$\frac{t}{q_t} = \frac{1}{k_2 q_2^2} + \frac{t}{q_2}$	(2)	q_2 (mmol g^{-1}) k_2 (g mmol^{-1} min^{-1})	[28,29]
Intraparticle diffusion model (IPD)	$q_t = k_{IPD} \cdot t^{0.5} + B$	(3)	B (mmol g^{-1}) k_{IPD} (mmol g-1 min$^{-0.5}$)	[28,30]
Liquid film diffusion model (LFD)	$ln(1 - F) = -k_{LFD} \cdot t$	(4)	$F = q_t/q_e$ (-) k_{LFD} (min^{-1})	[31,32]
Langmuir isotherm	$q_e = \frac{q_L \cdot k_L \cdot c_e}{1 + k_L \cdot c_e}$	(5)	q_L (mmol g^{-1}) k_L (dm^3 mmol^{-1})	[33,34]
Freundlich isotherm	$q_e = k_F \cdot c_e^{1/n}$	(6)	$1/n$ (-) k_F ((dm^3)$^{1/n}$ mmol$^{(1-1/n)}$ g^{-1})	[34,35]

where:

B parameter related to the thickness of the boundary layer (mmol g^{-1})

c_e equilibrium concentration of Ni(II) (mmol dm^{-3})

F fractional attainment of equilibrium (-)

k_1 rate constant of the PFO model (min^{-1})

k_2 rate constant of the PSO model (g mmol^{-1} min^{-1})

k_F Freundlich constant indicative of the relative adsorption capacity of the adsorbent ((dm^3)$^{1/n}$ mmol$^{(1-1/n)}$ g^{-1})

k_{IPD} intraparticle diffusion rate constant (mmol g^{-1} min^{-1})

k_L Langmuir constant related to the energy of adsorption (dm^3 mmol^{-1})

k_{LFD}	liquid film diffusion rate constant (min^{-1})
n	Freundlich equation exponent (-)
q_{exp}	amount of adsorbed Ni(II) obtained experimentally (mmol g^{-1})
q_1	adsorption capacity of Ni(II) for PFO model (mmol g^{-1})
q_2	adsorption capacity of Ni(II) for PSO model (mmol g^{-1})
q_e	amount of Ni(II) adsorbed at equilibrium (mmol g^{-1})
q_L	maximum adsorption capacity in the Langmuir model (mmol g^{-1})
q_t	amount of Ni(II) adsorbed at time t (mmol g^{-1})
t	time (min)
T	temperature (K)

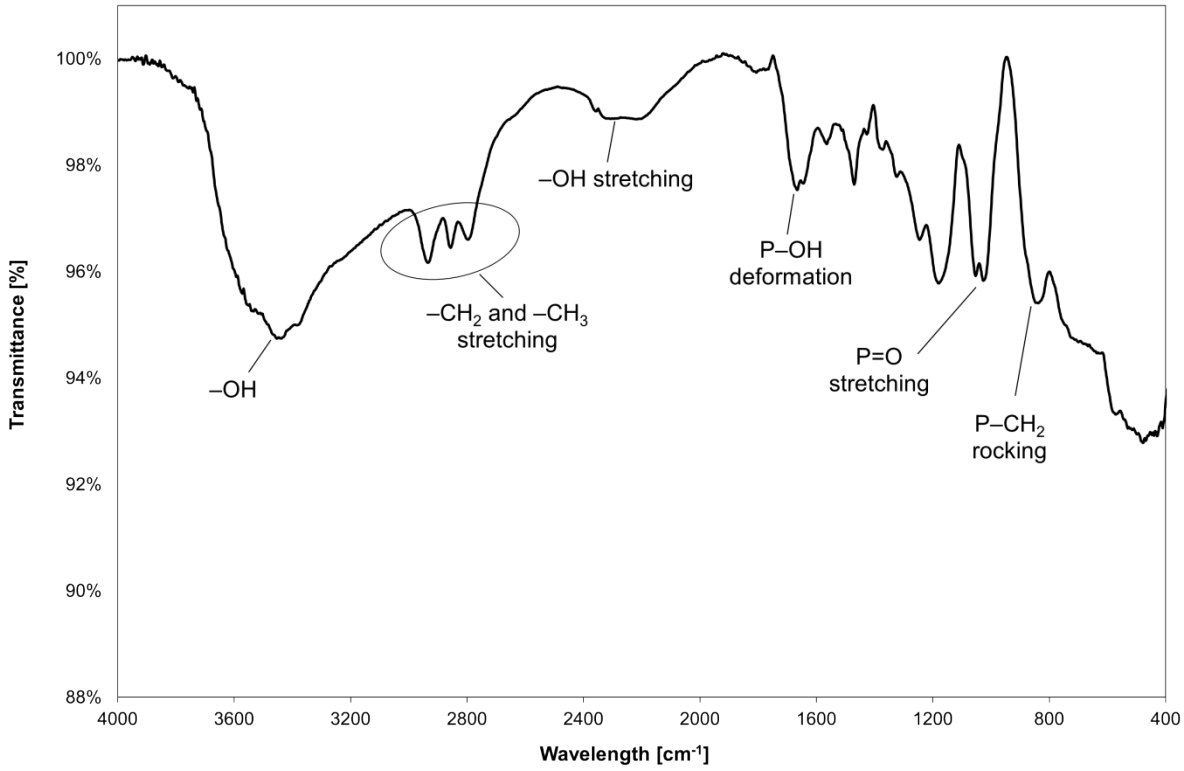

Fig. S1. FTIR spectrum of the obtained amino-hypophosphite polyampholyte with signal assignment (based on [36-38]).

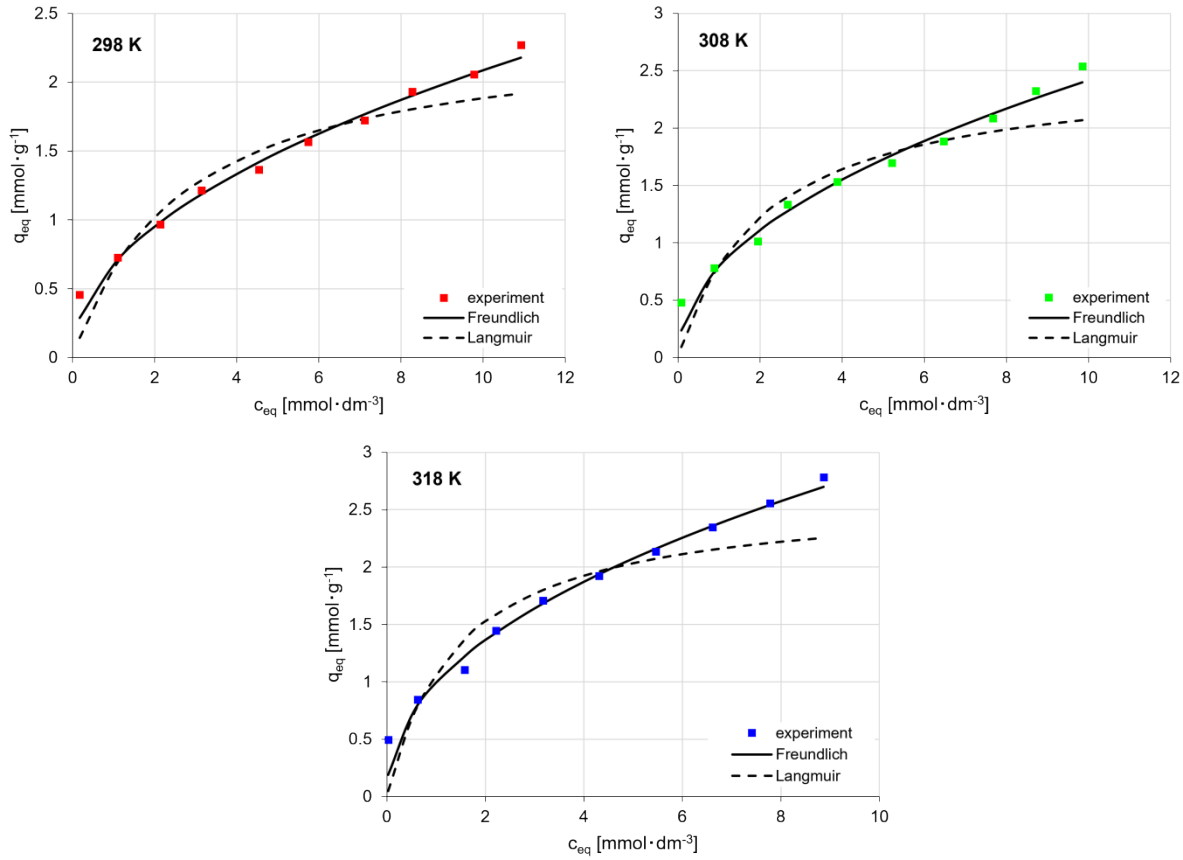

Fig. S2. Sorption isotherms of the obtained amino-hypophosphite polyampholyte for removal of Ni(II) in different temperature. Simulation by Freundlich and Langmuir models.

References

[1] Kołodyńska, D. (2009) Polyacrylate anion exchangers in sorption of heavy metal ions with the biodegradable complexing agent. Chem. Eng. J. 150, 280–288. https://doi.org/10.1016/j.cej.2008.12.027

[2] Bąk, J., Sofińska-Chmiel, W., Gajewska, M., Malinowska, P., Kolodyńska, D. (2023) Determination of the Ni(II) Ions Sorption Mechanism on Dowex PSR2 and Dowex PSR3 Ion Exchangers Based on Spectroscopic Studies. Materials 16(2): 644. https://doi.org/10.3390/ma16020644

[3] Silva, R.M.P.; Manso, J.P.H.; Rodrigues, J.R.; Lagoa, R. (2008) A comparative study of alginate beads and an ion-exchange resin for the removal of heavy metals from a metal plating effluent. J. Environ. Sci. Health Part A 43: 1311–1317. https://doi.org/10.1080/10934520802177953

[4] Wołowicz, A.; Hubicki, Z. (2016) Carbon-based adsorber resin Lewatit AF 5 applicability in metal ion recovery. Microporous Mesoporous Mater. 224: 400–414. https://doi.org/10.1016/j.micromeso.2015.12.051

[5] Wołowicz, A.; Wawrzkiewicz, M. (2021) Screening of Ion Exchange Resins for Hazardous Ni(II) Removal from Aqueous Solutions: Kinetic and Equilibrium Batch Adsorption Method. Processes 9(2): 285. https://doi.org/10.3390/pr9020285

[6] Wołowicz, A.; Hubicki, Z. (2012) The use of the chelating resin of a new generation Lewatit MonoPlus TP-220 with the bis-picolylamine functional groups in the removal of selected metal ions from acidic solutions. Chem. Eng. J. 197: 493–508. https://doi.org/10.1016/j.cej.2012.05.047

[7] Argun M.E. (2008) Use of clinoptilolite for the removal of nickel ions from water: kinetics and thermodynamics. J Hazard Mater. 150(3): 587-595. https://doi.org/10.1016/j.jhazmat.2007.05.008

[8] Kabuba J. and Banza M. (2021) Modification of clinoptilolite with dialkylphosphinicacid for the selective removal of cobalt (II) and nickel (II)from hydrometallurgical effluent. Can J Chem Eng. 99: S168–S178. DOI:10.1002/cjce.24005

[9] Dinu, M.V., Dragan, E.S. (2010) Evaluation of Cu2+, Co2+ and Ni2+ ions removal from aqueous solution using a novel chitosan/clinoptilolite composite: Kinetics and isotherms. Chem. Eng. J. 160: 157–163. https://doi.org/10.1016/j.cej.2010.03.029

[10] Wu, S.P., Dai, X.Z., Kan, J.R., Shilong, F.D., Zhu, M.Y. (2017) Fabrication of carboxymethyl chitosan–hemicellulose resin for adsorptive removal of heavy metals from wastewater. Chinese Chem. Lett. 28: 625–632. https://doi.org/10.1016/j.cclet.2016.11.015

[11] Jiang, C., Wang, X., Wang, G., Hao, C., Li, X., Li, T. (2019) Adsorption performance of a polysaccharide composite hydrogel based on crosslinked glucan/chitosan for heavy metal ions. Compos. Part B Eng. 169: 45–54. https://doi.org/10.1016/j.compositesb.2019.03.082

[12] Kandah M.I.; Meunier J.L. (2007) Removal of nickel ions from water by multi-walled carbon nanotubes. Journal of Hazardous Materials 146: 283–288. https://doi.org/10.1016/j.jhazmat.2006.12.019

[13] Cao, F., Lian, C., Yu, J., Yang, H., Lin, S. (2019) Study on the adsorption performance and competitive mechanism for heavy metal contaminants removal using novel multi-pore activated carbons derived from recyclable long-root Eichhornia crassipes. Bioresource Technology 276: 211–218. https://doi.org/10.1016/j.biortech.2019.01.007

[14] Di Natale, F., Gargiulo, V., Alfè, M. (2020) Adsorption of heavy metals on silica-supported hydrophilic carbonaceous nanoparticles (SHNPs). J. Hazard. Mater. 393: 122374. https://doi.org/10.1016/j.jhazmat.2020.122374

[15] Liu, L., Liu, S., Peng, H., Yang, Z., Zhao, L., Tang, A. (2020) Surface charge of mesoporous calcium silicate and its adsorption characteristics for heavy metal ions. Solid State Sci. 99: 106072. https://doi.org/10.1016/j.solidstatesciences.2019.106072

[16] Akpomie, K.G., Dawodu, F.A. (2016) Acid-modified montmorillonite for sorption of heavy metals from automobile effluent. Beni-Suef Univ. J. Basic Appl. Sci. 5: 1–12. https://doi.org/10.1016/j.bjbas.2016.01.003

[17] Es-Sahbany, H., Berradi, M., Nkhili, S., Hsissou, R., Allaoui, M., Loutfi, M., Bassir, D., Belfaquir, M., El Youbi, M.S. (2019) Removal of heavy metals (nickel) contained in wastewater-models by the adsorption technique on natural clay. Materials Today: Proceedings 13: 866–875. https://doi.org/10.1016/j.matpr.2019.04.050

[18] Vhahangwele, M., Mugera, G.W. (2015) The potential of ball-milled South African bentonite clay for attenuation of heavy metals from acidic wastewaters: Simultaneous sorption of Co2+, Cu2+, Ni2+, Pb2+, and Zn2+ ions. J. Environ. Chem. Eng. 3: 2416–2425. https://doi.org/10.1016/j.jece.2015.08.016

[19] Arshadi, M., Amiri, M.J., Mousavi, S. (2014) Kinetic, equilibrium and thermodynamic investigations of Ni(II), Cd(II), Cu(II) and Co(II) adsorption on barley straw ash. Water Resour. Ind. 6: 1–17. https://doi.org/10.1016/j.wri.2014.06.001

[20] Abdelfattah, I., Ismail, A.A., Sayed, F.Al, Almedolab, A., Aboelghait, K.M. (2016) Biosorption of heavy metals ions in real industrial wastewater using peanut husk as efficient and cost effective adsorbent. Environ. Nanotechnology, Monit. Manag. 6: 176– 183. https://doi.org/10.1016/j.enmm.2016.10.007

[21] Malik, R., Dahiya, S., Iata, S. (2017) An experimental and quantum chemical study of removal of utmostly quantified heavy metals in wastewater using coconut husk: A novel approach to mechanism. Int. J. Biol. Macromol. 98: 139–149. https://doi.org/10.1016/j.ijbiomac.2017.01.100

[22] Shooto, N.D., Dikio, E.D. (2018) Highly porous MOF adsorbent for wastewater treatment. Asian J. Chem. 30: 1723–1730. DOI:10.14233/ajchem.2018.21275

[23] Karami, H. (2013) Heavy metal removal from water by magnetite nanorods. Chem. Eng. J. 219: 209–216. https://doi.org/10.1016/j.cej.2013.01.022

[24] Ain, Q.U., Farooq, M.U., Jalees, M.I. (2020) Application of Magnetic Graphene Oxide for Water Purification: Heavy Metals Removal and Disinfection. J. Water Process Eng. 33: 101044. https://doi.org/10.1016/j.jwpe.2019.101044

[25] Lasheen, M.R., El-Sherif, I.Y., El-Wakeel, S.T., Sabry, D.Y., El-Shahat, M.F. (2017) Heavy metals removal from aqueous solution using magnetite Dowex 50WX4 resin nanocomposite. J. Mater. Environ. Sci. 8: 503–511.

[26] Almomani, F., Bhosale, R., Khraisheh, M., Kumar, A., Almomani, T. (2020) Heavy metal ions removal from industrial wastewater using magnetic nanoparticles (MNP). Applied Surface Science 506: 144924. https://doi.org/10.1016/j.apsusc.2019.144924

[27] Lagergren, S. (1898). Zur Theorie der sogenannten Adsorption gelöster Stoffe. Zeitschrift für Chemie und Industrie der Kolloide. Handlingar 24:1-24. https://doi.org/10.1007/BF01501332

[28] Qiu, H., L.V., Pan, B., Zhang, Q., Zhang, W., Zhang, Q. (2009). Critical review in adsorption kinetic models. Journal of Zhejiang University-SCIENCE A 10: 716-724. https://doi.org/10.1631/jzus.A0820524

[29] Ho, Y.S., McKay, G. (1999). Pseudo-second order model for sorption processes. Process Biochem. 34: 451-465.

[30] Weber Jr., W.J., Morris, J.C. (1963). Kinetics of adsorption on carbon from solution. J. Sanit. Eng. Div.-ASCE 89: 31-59. https://doi.org/10.1061/JSEDAI.0000430

[31] Boyd, G.E., Adamson, A.W., Myers Jr., L.S. (1947). The exchange adsorption of ions from aqueous solutions by organic zeolites. II. Kinetics. Journal of the American Chemical Society 69(11): 2836-2848. https://doi.org/10.1021/ja01203a066

[32] Tarawou, T., Young, E. (2015). Intraparticle and liquid film diffusion studies on the adsorption of Cu^{2+} and Pb^{2+} ions from aqueous solution using powdered cocoa pod (*Theobroma cacao*). International Research Journal of Engineering and Technology 2(8): 236-243.

[33] Langmuir, I. (1916). The constitution and fundamental properties of solids and liquids. J. Am., Chem. Soc. 38: 2221-2295. https://doi.org/10.1021/ja02268a002

[34] Wang, J., Guo, X. (2020). Adsorption isotherm models: Classification, physical meaning, application and solving method. Chemosphere 258: 127279. https://doi.org/10.1016/j.chemosphere.2020.127279

[35] Freundlich, H.M.F. (1906). Über die Adsorption Lösungen. Zeitschrift für Physikalische Chemie 57:385-470. https://doi.org/10.1515/zpch-1907-5723

[36] Fleming, I., Williams, D. (2019) Spectroscopic Methods in Organic Chemistry, Spectroscopic Methods in Organic Chemistry. Springer, Cham. https://doi.org/10.1007/978-3-030-18252-6_3

[37] Socrates, G. (2001) Infrared and Raman characteristic group frequencies. Tables and charts. Journal of Raman Spectroscopy, 3rd edition. ed.,. John Wiley & Sons.

[38] Yadav, L.D.S. (2005) Organic spectroscopy. Organic Spectroscopy. Springer, Netherlands. https://doi.org/10.1007/978-1-4020-2575-4.